

---

# The Model Knows, the Decoder Finds: Future Value Guided Particle Power Sampling

---

Tu Nguyen<sup>1</sup>   Rasul Tutunov<sup>2</sup>   Xiaotong Ji<sup>2</sup>   Matthieu Zimmer<sup>2</sup>

<sup>1</sup>Huawei Heisenberg Research Center

<sup>2</sup>Huawei Noah’s Ark Lab

{tu.nguyen, rasul.tutunov, matthieu.zimmer}@huawei.com

xiaotong.ji1@h-partners.com

## Abstract

A recurring pattern in “reasoning without training” is that base LLMs already assign non-trivial probability mass to correct multi-step solutions; the bottleneck is locating these modes efficiently at inference time. A principled way to bias inference toward such modes is *power sampling*, i.e., sampling from  $p_\theta(x)^\alpha$  with  $\alpha > 1$ . Recent work makes power sampling practical by estimating a future-dependent correction factor  $z_t$  via Monte Carlo rollouts, thereby replacing iterative Markov chain Monte Carlo with forward-looking estimation. In this paper, we reframe that correction factor as a *future-value selection potential* in a Sequential Monte Carlo (SMC) view of power sampling:  $z_t$  plays the role of a critic-like quantity, but can be estimated directly from the model by short-horizon rollouts, no verifier and no training required.

Building on this view, we introduce **Auxiliary Particle Power Sampling (APPS)**, a blockwise particle algorithm for training-free reasoning that approximates the sequence-level power target with a bounded population of partial solutions. APPS propagates these hypotheses in parallel by proposal-corrected power reweighting and refines their survival through future-value-guided selection at resampling boundaries, so that finite compute is redistributed across competing prefixes rather than spent along a single unfolding path. This yields a transparent scaling knob in the particle count, predictable peak memory, and a compute pattern that avoids both iterative trajectory editing and dense candidate-wise rollout fan-out, while improving robustness to pivotal early decisions by keeping multiple hypotheses alive throughout decoding. We further study an amortized variant in which the rollout-based selection potential is replaced by a lightweight learned head trained offline from rollout supervision, enabling fast future-value guidance at inference time. More broadly, our results add to a growing view that a nontrivial part of the gains often attributed to post-training may also be approached through more faithful power approximation at inference time.

## 1 Introduction

Large language models already contain many correct solutions: short proofs [Bai et al., 2023], clean derivations [Wei et al., 2022], and executable programs that pass tests [Chen et al., 2021b, Li et al., 2022]. The bottleneck is increasingly not capability, but reliability under finite inference. Long contexts [Liu et al., 2024, Hsieh et al., 2024], tight latency and memory budgets [Wu et al., 2025, Behnam et al., 2025], and locally plausible early decisions can quietly derail the remainder of a trajectory [Gao et al., Huang et al., 2025b]. This motivates a line of work that *treats reasoning as an inference-time search problem*: without changing model parameters, can we steer generation

toward higher-quality trajectories that already have nontrivial probability under the base model [Shao et al., 2024, Karan and Du, 2025, Ji et al., 2026]? A key insight is that the difficulty is not just in *proposing* good continuations, but in *selecting* which partial solutions deserve continued computation: a decision that depends on futures the decoder has not yet seen.

**From local sharpening to sequence-level targets.** A natural training-free idea is to sharpen the model distribution. Low-temperature sampling concentrates mass locally, but it remains myopic: it increases the probability of high-confidence next tokens without correcting for errors that only become visible many steps later. Sequence-level methods instead target a globally sharpened power distribution over complete trajectories,  $\pi_\alpha(x) \propto p(x)^\alpha$  with  $\alpha > 1$ . Best-of- $N$  partially approximates this goal by selecting among independent samples, but selection under base-model likelihood is only an indirect proxy for  $\pi_\alpha$ . MCMC power sampling targets  $\pi_\alpha$  more directly in the limit, but can incur substantial wall-clock overhead because each step repeatedly regenerates suffixes [Karan and Du, 2025]. Recent scalable alternatives replace iterative MCMC mixing with explicit lookahead rollouts, improving finite-budget behavior but relocating the burden of inference to decision points, where branching becomes costly as contexts lengthen and batching tightens [Ji et al., 2026].

**Why future value matters.** A core difficulty in approximating  $\pi_\alpha$  is that the quality of a prefix is not determined by its immediate likelihood alone. For a prefix  $x_{1:t}$ , the remaining mass under the power distribution depends on a suffix normalizer

$$z_t(x_{1:t}) = \sum_{x_{t+1:T}} p(x_{t+1:T} | x_{1:t})^\alpha,$$

whose log is a long-horizon future value: it measures how much power-weighted probability mass remains reachable from the current state. Prefix-only reweighting can therefore be unstable at finite compute. It may eliminate prefixes that look slightly worse locally but retain larger  $z_t$ , and it may over-amplify prefixes that are locally sharp yet lead into dead ends. The central question is therefore: can we inject a tractable estimate of  $z_t$  into finite-budget inference *without* training a separate value model, and if so, *where* in the inference algorithm does it yield the largest gain per unit of compute?

**Our stance: preserve many presents, and select by reachable futures.** We take a population-based view in which future value becomes explicit precisely where finite-budget inference must decide what continues to receive mass. Rather than repeatedly unfolding many futures from a single prefix, which can be costly in Ji et al. [2026], we maintain a bounded population of prefixes that evolve together and compete over time. At resampling boundaries, selection is guided by reachable power-weighted mass: prefixes with stronger downstream promise retain representation, while collapsed regions relinquish it. In this way, APPS casts finite-budget decoding as a controlled redistribution of probability mass across competing partial trajectories. Its minimal form already instantiates this view; rollout and learned selection potentials refine the same selection law with increasingly explicit estimates of downstream value.

**Auxiliary Particle Power Sampling.** We introduce APPS, a training-free and verifier-free algorithm for approximating power distributions under a finite particle budget. APPS evolves a bounded population of partial trajectories in blocks of tokens, combining proposal-corrected weighting with weighted selection across prefixes. The key observation is that, under the global power target, the merit of a candidate block is not exhausted by its immediate likelihood: it also depends on the power-weighted mass of the continuations that remain reachable after committing to it. APPS is organized around this boundary law. Propagation stays local, while selection carries the long-horizon signal that determines which prefixes survive under finite compute.

**Relation to concurrent baselines.** Our approach is complementary to recent rollout-based and particle-based approximations. Scalable power sampling [Ji et al., 2026] emphasizes explicit future correction at decision points, while Power SMC [Azizi et al., 2026] shows how far a prefix-optimal particle backbone can go when control enters primarily through the proposal. APPS shares the particle perspective but locates its primary contribution at a different point in the algorithm: not in the proposal, but in *selection-time future-value guidance*. The proposal remains simple and stable; what changes is how finite population mass is redistributed at boundaries, informed by estimated downstream promise. This makes the two approaches naturally complementary: future-value selection potentials could in principle be combined with richer proposals.

**Amortized future value.** Rollouts make the hidden future of a prefix momentarily visible, but only at substantial cost. We therefore compress this lookahead signal into a lightweight boundary-level head. In this way, APPS need not repeatedly simulate the future in order to sense it: a cheap predictor carries the same downstream signal into selection, while the base language model remains unchanged.

**Contributions.** In summary, we contribute:

- **APPS.** A particle-based, verifier-free decoding algorithm that approximates power distributions with a finite inference budget through blockwise proposal-corrected weighting and adaptive resampling.
- **Selection-time future value.** A principled use of short-horizon rollouts to estimate the suffix normalizer  $z_t$  and inject it only at resampling, refining how finite population mass is redistributed while leaving the proposal-corrected propagation law unchanged.
- **Finite-budget population allocation.** A particle-based inference view in which resampling also governs where computation continues to flow over time, coupling effectiveness and efficiency within the same selection law.
- **Learned future-value distillation.** A lightweight boundary-level head that amortizes the rollout-based selection potential from hidden states, reducing online rollout cost while preserving the same value-aware selection principle.
- **Empirical accuracy–runtime trade-offs.** Across challenging reasoning benchmarks, APPS delivers competitive accuracy with favorable runtime behavior. The core sampler already performs strongly, while explicit future-value selection—via rollout or learned potentials—provides further gains in regimes where downstream value is especially informative.

## 2 Preliminaries

**A distributional view of decoding.** A pretrained language model does not merely *score* text; it defines a distribution over possible continuations, and decoding is the rule by which we move through that distribution. Fix a prompt  $x$ , and let  $y$  denote a full completion. The model assigns an autoregressive likelihood  $p(y | x)$ , which we may regard as the native plausibility of a trajectory under the base model. Our aim is to change the *walk* without changing the *landscape*: we keep  $p$  fixed and modify only the inference procedure, so that trajectories the model already considers plausible become easier to recover under finite computation.

**The sequence-level power target.** To bias decoding toward what the model already believes, we sharpen its distribution at the level of whole trajectories:

$$p^{(\alpha)}(y | x) \propto p(y | x)^\alpha, \quad \alpha > 1. \quad (1)$$

When correct solutions exist as low-probability but genuine modes under  $p$ , the power target makes them easier to recover by concentrating probability mass around higher-likelihood trajectories. This differs from low-temperature decoding, which sharpens only local conditionals; sequence-level power sampling is global, and therefore depends not only on how good a move looks now, but also on what that move preserves downstream.

**Future value at block boundaries.** Because our method operates in *blocks*, we work at block granularity. Fix a block size  $B$  and write a completion as a sequence of blocks  $b_{1:j}$ . Let  $\pi^{(\alpha)}(b_{1:j} | x)$  denote the induced sequence-level power target, and for a boundary  $j$ , let  $\pi_j^{(\alpha)}(\cdot | x, b_{<j})$  denote the corresponding next-block conditional. Then

$$\pi_j^{(\alpha)}(b_j | x, b_{<j}) \propto p(b_j | x, b_{<j})^\alpha z_{j+1}(x, b_{1:j}), \quad (2)$$

where  $z_{j+1}(x, b_{1:j})$  is the remaining power-weighted mass of all suffixes after appending  $b_j$ . This suffix-value term is the exact measure of *future value*: it quantifies how much power-weighted continuation mass remains reachable after committing to the current block. Thus, local power sharpening is not the whole story. The correct boundary law is tilted by what the current choice still keeps alive.

**Particle approximation under finite computation.** The difficulty is that  $z_{j+1}(x, b_{1:j})$  is intractable to compute exactly. A natural approximation strategy is therefore population-based: maintain a set of partial trajectories, advance them forward, update their weights, and occasionally resample so that computation remains focused on prefixes that still matter. This yields a blockwise sequential Monte Carlo approximation to the power target. The main failure mode is population collapse: after a few steps, most of the mass may concentrate on only a few particles, leaving the rest effectively irrelevant. We monitor this using effective sample size (ESS). If  $\{\bar{w}^{(i)}\}_{i=1}^P$  are normalized particle weights, then

$$\text{ESS} = \frac{1}{\sum_{i=1}^P (\bar{w}^{(i)})^2}, \quad (3)$$

which decreases as the population becomes more concentrated. When ESS falls below a threshold, we resample and reallocate computation toward prefixes carrying the bulk of the mass.

**What APPS adds.** Our method is a blockwise particle approximation to the power target in (1). The minimal sampler uses proposal-corrected blockwise weights, so that practical decoding proposals still represent the same sharpened sequence-level target. What remains missing is the future-value term in (2). APPS addresses this by introducing a *selection potential*: a computable proxy for suffix value that enters only through selection, refining which prefixes survive and how offspring are allocated, while leaving proposal and propagation unchanged.

### 3 Methodology: Auxiliary Particle Power Sampling

The minimal requirement for approximating the power target  $\pi_\alpha(y | x) \propto p(y | x)^\alpha$  under finite compute is a population of partial trajectories whose weights reflect the sequence-level objective. The central difficulty, however, is that prefix likelihood alone does not determine a prefix's value under  $\pi_\alpha$ : the correct boundary law also depends on the power-weighted mass of all continuations still reachable. We begin by making this dependence precise, then describe the particle backbone that targets the power objective, and finally introduce the future-value selection potentials that form the main contribution of this work.

#### 3.1 The power target and its future-value factorization

Fix a prompt  $x$ , a finite block horizon  $J$ , and a countable block space. A full completion is a sequence of blocks  $b_{1:J} := (b_1, \dots, b_J)$ . Define the unnormalized sequence-level power target

$$\gamma_J(b_{1:J} | x) := \prod_{k=1}^J p(b_k | x, b_{<k})^\alpha, \quad \pi_J(b_{1:J} | x) := \frac{\gamma_J(b_{1:J} | x)}{Z_J(x)}, \quad (4)$$

where  $Z_J(x) := \sum_{b_{1:J}} \gamma_J(b_{1:J} | x)$ . For  $j \in \{1, \dots, J\}$ , define the prefix mass

$$\gamma_j(b_{1:j} | x) := \prod_{k=1}^j p(b_k | x, b_{<k})^\alpha,$$

and the suffix value

$$z_{j+1}(x, b_{1:j}) := \sum_{b_{j+1:J}} \prod_{k=j+1}^J p(b_k | x, b_{<k})^\alpha,$$

with the convention  $z_{J+1} \equiv 1$ . The following theorem isolates the exact role of future value at every block boundary.

**Theorem 1** (Future-value factorization). *For every block boundary  $j$ , the  $j$ -prefix marginal of the power target satisfies*

$$\pi_{1:j}(b_{1:j} | x) = \frac{\gamma_j(b_{1:j} | x) z_{j+1}(x, b_{1:j})}{Z_J(x)}. \quad (5)$$

Consequently, for every fixed prefix  $b_{<j}$ , the next-block conditional is

$$\pi_j(b_j | x, b_{<j}) = \frac{p(b_j | x, b_{<j})^\alpha z_{j+1}(x, b_{1:j})}{z_j(x, b_{<j})} \propto p(b_j | x, b_{<j})^\alpha z_{j+1}(x, b_{1:j}). \quad (6)$$

*Proof.* Appendix C.1 gives the full derivation. The key step is to split the product  $\gamma_j$  into a prefix factor  $\gamma_j$  (constant w.r.t. the suffix sum) and a suffix factor whose marginal is  $z_{j+1}$ ; dividing adjacent prefix marginals then yields (6).  $\square$

**Interpretation.** Equation (6) decomposes the true block-boundary law into two factors. The first,  $p(b_j \mid x, b_{<j})^\alpha$ , is the local power-weighted preference for the next block: it is computable from logits alone. The second,  $z_{j+1}(x, b_{1:j})$ , measures how much power-weighted continuation mass remains reachable after committing to that block. Future value is therefore not an auxiliary heuristic: it is exactly the correction that turns local power weighting into the true boundary marginal. An algorithm that reweights by prefix likelihood alone implicitly sets  $z_{j+1} \equiv \text{const}$ , which can be severely wrong when locally strong prefixes lead into regions of low continuation quality.

**Finite-budget approximation.** Theorem 1 identifies the exact boundary law; the next result characterizes how well a finite particle population can approximate it. Consider  $P$  particles drawn i.i.d. from a proposal  $q_j$  and reweighted by the self-normalized importance ratio  $r(b_j) := \pi_j(b_j)/q_j(b_j)$ .

**Theorem 2** (Bounded-test particle approximation). *For every bounded measurable  $f$  with  $\|f\|_\infty \leq 1$ , the self-normalized importance-sampling estimator  $\hat{\pi}_j^P(f) := \sum_{i=1}^P \bar{w}_i f(X_i)$  satisfies*

$$\mathbb{E}[|\hat{\pi}_j^P(f) - \pi_j(f)|] \leq \frac{4}{\sqrt{P}} \sqrt{1 + \chi^2(\pi_j \| q_j)} + \frac{8}{P} \chi^2(\pi_j \| q_j). \quad (7)$$

*Proof.* See Appendix C.2.

The key quantity controlling approximation quality is the  $\chi^2$ -divergence  $\chi^2(\pi_j \| q_j)$ . When the proposal  $q_j$  is close to the target  $\pi_j$ , the divergence is small and moderate  $P$  suffices; when the two disagree, in particular when  $z_{j+1}$  varies widely across blocks and the proposal ignores it, the divergence grows and more particles are needed. This sets up the central question for Section 3.3: can we reduce  $\chi^2(\pi_j \| q_j)$  without changing the proposal, by instead modifying which particles survive at resampling?

### 3.2 Blockwise particle backbone

The factorization above (Equation 6) motivates a two-part approximation strategy: a particle population whose weights track the local power factor, and a selection mechanism that accounts for the future-value factor. We describe the first part here and the second in Section 3.3.

APPS maintains  $P$  partial trajectories (particles), with time measured in blocks of  $B$  tokens. At stage  $j$ , each particle  $i$  proposes a next block from a tractable proposal,

$$[b_j]^{(i)} \sim q_j(\cdot \mid x, [b_{<j}]^{(i)}),$$

and receives the incremental log-weight

$$\Delta \log w_j^{(i)} = \alpha \log p([b_j]^{(i)} \mid x, [b_{<j}]^{(i)}) - \log q_j([b_j]^{(i)} \mid x, [b_{<j}]^{(i)}). \quad (8)$$

This identity separates *exploration* (the proposal) from *representation* (the power target): both log-terms are computed from logits already produced during generation, and when the proposal uses truncation or temperature,  $\log q_j$  is the renormalized likelihood of the sampled tokens. A natural proposal aligns with the locally sharpened model (e.g., temperature  $\tau < 1$ ), keeping the correction in (8) stable.

As noted in Corollary 1 (Appendix C.4), the cumulative product of these incremental weights equals the standard importance ratio for  $\gamma_j/q$ , so the backbone already defines a valid blockwise importance-sampling construction for the sequence-level power target (even before any future-value correction is introduced).

**Resampling and population control.** After several blocks, particle mass typically concentrates: a few prefixes carry most of the weight while many contribute little. APPS monitors this via effective sample size,

$$\text{ESS} = \frac{1}{\sum_{i=1}^P (\bar{w}^{(i)})^2}, \quad (9)$$

and resamples when  $\text{ESS} < \kappa P$ . At resampling, descendant indices are drawn from the current selection scores (Section 3.3), and a separate cumulative ancestry score is propagated through sampled parent indices for final particle selection; this keeps local resampling numerically stable while preserving a trajectory-level ranking across resampling events. Under *dynamic allocation*, the active population size is additionally adapted via a boundary-level ambiguity score (Appendix E.1).

### 3.3 Future-value selection potentials

The backbone of Section 3.2 captures the local power factor  $p(b_j \mid x, b_{<j})^\alpha$  through proposal-corrected weighting. What it does *not* capture is the future-value factor  $z_{j+1}$  in the true boundary law (6). At finite particle count, this omission can cause premature collapse: the population concentrates on prefixes that look strong locally but whose continuations are poor.

APPS addresses this by introducing a computable *selection potential*  $\psi_j^{(i)} \approx z_{j+1}(x, [b_{1:j}]^{(i)})$  that enters the algorithm *only* at resampling. At each boundary where resampling is triggered, we form augmented selection weights

$$\log \tilde{w}_j^{(i)} = \log w_j^{(i)} + \eta \log \psi_j^{(i)}, \quad (10)$$

where  $\eta > 0$  controls the strength of the future-value signal. Selection probabilities and expected offspring are then

$$\rho_j^{(i)} := \frac{\tilde{w}_j^{(i)}}{\sum_{k=1}^{P_j} \tilde{w}_j^{(k)}}, \quad \mathbb{E}[N_j^{(i)} \mid \{\tilde{w}_j^{(k)}\}] = P_j^+ \rho_j^{(i)}, \quad (11)$$

where  $N_j^{(i)}$  is the offspring count and  $P_j^+$  is the post-resampling population size. Thus future value enters the particle system through expected offspring allocation: prefixes with stronger downstream promise retain representation, while collapsed regions relinquish it. Proposal and propagation remain unchanged; the selection potential acts only through resampling.

**Why selection is the right injection point.** In a finite particle system, future value matters only insofar as it changes which branches survive and how many descendants they leave. Modifying the *proposal* to depend on  $z_{j+1}$  would require evaluating the intractable suffix normalizer *before* sampling each token: it would be too expensive. Modifying *post-hoc filtering* (e.g., Best-of- $N$ ) discards all intermediate structure. Selection-time injection is the minimal intervention: it preserves the stable, local proposal while redirecting finite population mass toward prefixes whose futures remain globally promising.

**Theoretical benefit: variance reduction from selection potentials.** The following proposition formalizes the intuition that a selection potential correlated with the true suffix normalizer reduces the particle count needed for a given approximation quality.

**Proposition 1** (Variance reduction from future-value selection). *Consider self-normalized importance sampling at block boundary  $j$  with  $P$  particles, proposal  $q_j$ , and target  $\pi_j(b_j) \propto p(b_j \mid x, b_{<j})^\alpha z_{j+1}(x, b_{1:j})$ . Suppose resampling uses augmented weights  $\tilde{w}^{(i)} \propto w^{(i)} \psi^{(i)}$  with a strictly positive selection potential  $\psi$ , and define the effective proposal*

$$\tilde{q}_j(b_j) := \frac{q_j(b_j) \psi(b_j)}{\sum_{b'} q_j(b') \psi(b')}. \quad (12)$$

*Then the approximation error at this boundary is governed by  $\chi^2(\pi_j \parallel \tilde{q}_j)$  in place of  $\chi^2(\pi_j \parallel q_j)$ , via Theorem 2. Writing  $r(b_j) := \pi_j(b_j)/q_j(b_j)$ , we have the exact identity:*

$$1 + \chi^2(\pi_j \parallel \tilde{q}_j) = \mathbb{E}_{q_j}[r(b_j)^2] - \text{Cov}_{q_j}\left(\psi(b_j), \frac{r(b_j)^2}{\psi(b_j)}\right). \quad (13)$$

*Therefore,  $\chi^2(\pi_j \parallel \tilde{q}_j) < \chi^2(\pi_j \parallel q_j)$  if and only if*

$$\text{Cov}_{q_j}\left(\psi(b_j), \frac{r(b_j)^2}{\psi(b_j)}\right) > 0. \quad (14)$$

*In the ideal limit where  $\psi(b_j) \propto r(b_j)$ , this covariance attains its theoretical maximum, perfectly canceling the variance term and reducing the  $\chi^2$ -divergence to 0.*

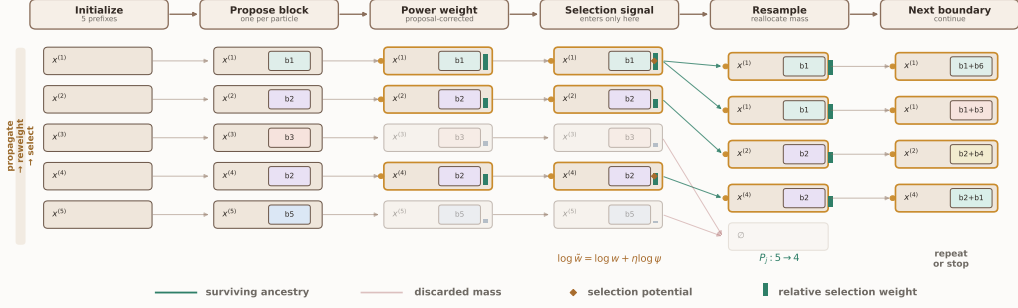


Figure 1: **Visual overview of APPS at a resampling boundary.** Five particle prefixes are propagated blockwise, *reweighted* under the sequence-level power target, and then *selected* under a finite particle budget. *Future-value selection potentials*, when active, refine only the selection weights. The example also illustrates *dynamic allocation*, with the active population shrinking from  $P_j = 5$  to  $P_{j+1} = 4$  before decoding continues.

**Interpretation.** The proposition provides a direct mathematical mechanism by which future-value selection *reduces the effective particle requirement*. The bound in Theorem 2 scales as  $O(P^{-1/2} \sqrt{1 + \chi^2})$ : replacing the baseline proposal with the augmented effective proposal reduces this penalty by exactly the statistical covariance between the injected potential  $\psi$  and the residual discrepancy  $r^2/\psi$ .

Intuitively, if the potential  $\psi$  successfully identifies prefixes with large missing future value ( $r$ ), both terms in the covariance move together: the assigned potential  $\psi$  is high, and the remaining ratio  $r^2/\psi$  (which scales with  $r$ ) is also high, yielding a strictly positive covariance value. When  $\psi$  perfectly matches the optimal trajectory mass  $r(b_j) \propto p(b_j)^\alpha z_{j+1}(b_j)/q_j(b_j)$ , this covariance perfectly counters the base variance, corresponding to zero-variance adapted importance sampling where  $\chi^2(\pi_j \parallel \hat{q}_j) = 0$ . Practical estimators operate between these extremes: any surrogate—such as a short rollout—that scales proportionally with the true downstream value  $z_{j+1}$  will induce a positive covariance and improve sample efficiency, avoiding the need for an exact internal value model.

**Rollout selection potential.** The first realization constructs  $\psi_j^{(i)}$  directly from sampled continuations. For each active particle  $i$  at boundary  $j$ , we launch  $R$  short lookahead rollouts of horizon  $H$  from  $[b_{1:j}]^{(i)}$ , score each by its power-weighted suffix quality, and aggregate:

$$\log \psi_j^{(i)} \approx \text{LME}_{r=1}^R s_{j,r}^{(i)}, \quad (15)$$

where LME denotes log-mean-exp and  $s_{j,r}^{(i)}$  is the rollout suffix score. This yields a *critic-free* estimate of downstream promise: future value is inferred from the model’s own continuations rather than from a separately trained value function. By Proposition 1, any positive correlation between this estimate and the true  $z_{j+1}$  reduces approximation error relative to the  $\psi \equiv 1$  baseline.

The cost of rollout APF is confined to resampling boundaries:

$$O(P_j^{\text{amb}} R H) \quad \text{per boundary,}$$

where  $P_j^{\text{amb}} \leq P_j$  is the number of ambiguous particles selected for lookahead (under dynamic allocation, not all particles require evaluation). The rollouts are short ( $H \ll B$ ), independent across particles, and batched; they do not modify the proposal or the KV caches used for continued generation.

**Learned selection potential.** The same boundary-level signal can be amortized. Let  $h_j^{(i)} \in \mathbb{R}^d$  denote the final-layer hidden state at the end of prefix  $i$  at boundary  $j$ . A lightweight MLP head  $f_\theta : \mathbb{R}^d \rightarrow \mathbb{R}$  predicts

$$\log \psi_j^{(i)} = f_\theta(h_j^{(i)}). \quad (16)$$

The head is trained offline to reproduce the within-boundary competition induced by rollout APF: which prefixes retain representation and in what proportions (Appendix D gives training details). At

inference time, it replaces explicit lookahead with a single forward pass per boundary, reducing the per-boundary cost from  $O(P_j^{\text{amb}}RH)$  to  $O(P_j)$ . Because the head is trained to predict the effective rollout signal rather than raw suffix values, it preserves the relative ranking that drives offspring allocation through (11), and Proposition 1 applies whenever its predictions are positively correlated with  $z_{j+1}$ .

**Cost summary.** The total cost of APPS decomposes cleanly. Propagation over block  $j$  costs  $O(P_jB)$ . Resampling without a selection potential adds negligible overhead. With rollout or learned potentials, the additional cost per triggered boundary is  $O(P_j^{\text{amb}}RH)$  or  $O(P_j)$ , respectively. In streaming mode, peak memory is dominated by the KV caches of the  $P_{\text{max}}$  active particles. Dynamic allocation (Appendix E.1) further reduces average compute by shrinking the active population at boundaries where selection has already converged.

## 4 Experiments

We study four questions: (Q1) how APPS compares with recent training-free power-sampling baselines under practical inference budgets; (Q2) when explicit future-value guidance improves over *p-only APPS*, i.e., the base sampler with proposal-corrected power weighting only and no auxiliary future-value selection potential; (Q3) whether a learned selection potential can recover the rollout signal; and (Q4) how *dynamic allocation* changes the accuracy–compute trade-off under a fixed particle budget. Unless noted otherwise, all results are single-seed, full-benchmark evaluations with identical prompts and task evaluators.

**Benchmarks.** We evaluate on three complementary reasoning benchmarks: **MATH500** [Lightman et al., 2023], scored by exact match on the extracted final answer; **HumanEval** [Chen et al., 2021a], scored by functional correctness under the standard unit tests; and **GPQA-diamond** [Rein et al., 2024], scored by exact match on the extracted answer in  $\{A, B, C, D\}$ . We use `pass@1` throughout.

**Models and APF training data.** Consistent with prior work, we study three 7B model families: *Qwen2.5-Math-7B*, *Qwen2.5-7B*, and *DeepSeek-Math-7B*. For learned selection potentials, we train a lightweight APF head on 14,468 rollout-labeled prompt–answer pairs from a mixed reasoning corpus: 45% BBH [Suzgun et al., 2022], 45% GSM8K [Cobbe et al., 2021], and 10% MATH [Hendrycks et al., 2021], with the MATH portion drawn from the full corpus but excluding MATH500 [Lightman et al., 2023]. This yields broad task coverage across reasoning domains while keeping training data disjoint from evaluation. Table 1 reports completed runs under a common protocol, including *p-only APPS*, APPS with rollout selection potential, and learned selection potential where available.

**Baselines and protocol.** We compare against the training-free baselines used in recent power-sampling work: standard decoding, low-temperature decoding, Best-of- $N$  [Brown et al., 2024], MH-MCMC power sampling [Karan and Du, 2025], and scalable power sampling [Ji et al., 2026]. As a post-training reference, we report the GRPO numbers from Ji et al. [2026], based on the checkpoint of Shao et al. [2025]. For published baselines, we retain the original protocols and numbers.

We additionally show Power SMC [Azizi et al., 2026] as reference points in the runtime plots where comparable results are available, but omit it from Table 1 to keep the main comparison on a uniform grid: the published results focus on MATH500 in a latency-oriented setting and do not cover the full HumanEval/GPQA grid reported here.

For APPS, we fix a dataset-specific block schedule across all models, variants, and particle budgets:  $B = 192$  for **MATH500**,  $B = 16$  for **HumanEval**, and  $B = 64$  for **GPQA**. This keeps APPS in a comparable practical compute regime to prior power-sampling baselines while reflecting that APPS updates its particle population at block boundaries. Unless noted otherwise, APPS runs use *dynamic allocation*, with  $\alpha = 4$ ,  $T_{\text{max}} = 3072$ , EOS termination, particle budgets  $N \in \{8, 16, 32\}$ , and a fixed APF strength  $\eta$  chosen on held-out development runs;  $N$  denotes the particle-budget cap. Rollout APF uses two short rollouts per APF call, evaluated only at selected resampling events. When a baseline is reported under a different budget or decoding setting, we retain the published number and mark the mismatch explicitly.

**APPS variants and ablation structure.** We treat the base particle sampler with proposal-corrected power weighting only (**p-only**) as the ablation baseline: it validates that the blockwise SMC backbone targets the correct sequence-level objective, but does not use any future-value signal at selection

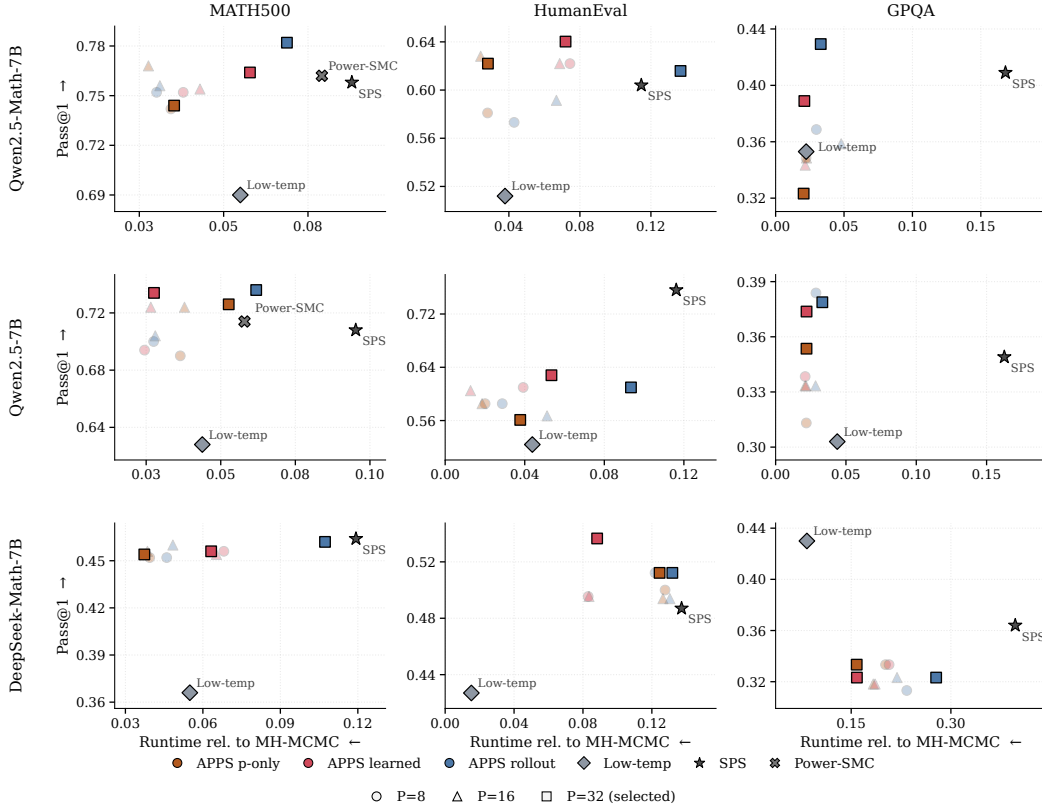


Figure 2: **Runtime–accuracy frontiers across three 7B models.** Each point shows the highest-pass@1 valid run within a method family at particle count  $P \in \{8, 16, 32\}$ ; square markers denote the selected  $P = 32$  operating points reported in Table 1. The plot is read as a Pareto-style comparison, with runtime normalized by a local MH-MCMC reference and preferred directions indicated by the axis arrows ( $\leftarrow$  lower wall-clock,  $\uparrow$  higher pass@1). Across models, **APPS (p-only)** is usually the fastest APPS variant, while **APPS (rollout APF)** often delivers the strongest accuracy, most clearly on MATH500 and in the strongest GPQA runs. At the same time, **APPS (learned APF)** frequently tracks rollout closely while remaining more runtime-efficient, making it a practical proxy for rollout guidance on HumanEval and GPQA. With value-guided selection, dynamic allocation, and finite-sample resampling, increasing the particle cap  $P$  need not monotonically improve the runtime–accuracy operating point; the best empirical point can occur below the largest budget.

time. The two future-value variants constitute the main experimental conditions: **APPS + rollout selection potential**, which adds short-rollout downstream-value estimates at resampling boundaries, and **APPS + learned selection potential**, which replaces explicit lookahead with a lightweight MLP head evaluated at the same boundaries. Comparing the future-value variants against p-only isolates the effect of the selection potential; comparing rollout against learned isolates the effect of amortization. Across all three conditions, the base model, prompts, evaluators, and decoding setup are fixed; only the resampling weights change.

#### 4.1 Main results across model families

Table 1 summarizes the validated results under the protocol above and gives the main empirical picture for **Q1–Q4**. It reports a common  $P = 32$  slice for all APPS variants, matching the operating points highlighted in Figure 2. This fixed-budget view avoids mixing APPS runs selected at different particle counts and makes the comparison between p-only, learned APF, and rollout APF direct.

For **Q1**, APPS remains competitive with recent training-free power-sampling baselines across all three model families. The p-only variant is a strong speed-oriented baseline: it has the lowest APPS overhead and is often close to the best training-free methods. However, the updated results also show

that explicit future-value guidance can materially improve the frontier. In particular, the strongest APPS points on Qwen2.5-Math-7B and Qwen2.5-7B often come from APF-guided variants rather than from p-only sampling.

For **Q2** and **Q3**, the clearest conclusion is not that one APF mechanism uniformly dominates, but that learned and rollout APF expose complementary regimes. Rollout APF gives the strongest APPS accuracy on several key slices: Qwen2.5-Math-7B on MATH500 and GPQA, Qwen2.5-7B on MATH500 and GPQA, and DeepSeek-Math-7B on MATH500. This confirms that online future-value estimates can be highly effective when the rollout signal is aligned with final correctness. Learned APF, by contrast, is the more stable and runtime-efficient proxy for that signal. It gives the best APPS result on HumanEval for Qwen2.5-Math-7B and DeepSeek-Math-7B, remains second-best or competitive in several GPQA and MATH500 settings, and occupies favorable runtime–accuracy regions in Figure 2. Thus, learned APF should be read less as a universally stronger oracle than rollout APF, and more as an amortized estimator that often captures much of the value of rollout guidance at lower variance and lower online cost.

The resulting hierarchy is task- and model-dependent. P-only is the most efficient APPS baseline and is hard to beat under tight compute. Rollout APF can deliver the highest accuracy, especially on MATH500 and the strongest GPQA runs, but its gains are less uniform because it relies on finite-sample, finite-horizon estimates made only at selected resampling events. Learned APF is generally the safer practical mechanism: it often tracks rollout quality while avoiding repeated online lookahead, which is especially valuable on HumanEval and GPQA. The DeepSeek results are more mixed than the Qwen results. One likely factor is completion length: on GPQA, DeepSeek outputs are much shorter than Qwen outputs, with median length only 27 characters versus roughly 1.5k for Qwen2.5-7B and 1.8k for Qwen2.5-Math-7B, leaving limited room for branching and resampling to affect the final answer.

For **Q4**, the evidence is favorable but nuanced. Several strong APPS operating points remain competitive at fixed  $P = 32$ , so dynamic allocation is not required for APPS to be useful. At the same time, the runtime plots show that adaptive population control can improve efficiency when uncertainty is heterogeneous across prefixes, by concentrating particles on unresolved branches rather than spending the full budget uniformly throughout decoding. We therefore view dynamic allocation as a compute-control mechanism rather than a universally dominant ingredient: its benefit depends on how unevenly uncertainty is distributed during generation.

## 5 Conclusion

We introduced APPS, a training-free framework for particle power sampling that brings post-training-style gains closer to base-decoding efficiency. By separating proposal-corrected propagation from selection-time future-value guidance, APPS yields a strong minimal sampler that already operates near the speed of base decoding, while rollout and learned selection potentials further improve how finite inference-time compute is deployed. Empirically, this places APPS in the narrow but important regime between decoding and post-training: substantially more accurate than standard decoding, often competitive with or stronger than recent training-free baselines, and in selected settings surprisingly close to post-trained performance without modifying model weights. More broadly, our results suggest that some of the benefits often attributed to post-training can instead be recovered at inference time, provided the decoder is allowed to maintain, weight, and selectively preserve multiple possible futures.

Table 1: **Training-free sampling results across three 7B models at fixed particle budget  $P = 32$ .** We compare Qwen2.5-Math-7B, Qwen2.5-7B, and DeepSeek-Math-7B on MATH500, HumanEval, and GPQA. Best and second-best *training-free* entries within each model–dataset pair are highlighted; APPS rows correspond to the  $P = 32$  operating points shown in the runtime–accuracy figures.

Method	MATH500	HumanEval	GPQA
<b>Qwen2.5-Math-7B</b>			
Base decoding [Ji et al., 2026]	0.496	0.329	0.278
Low-temp ( $\tau = 1/\alpha$ ) [Ji et al., 2026]	0.690	0.512	0.353
Best-of- $N$ ( $N = 32$ ) [Ji et al., 2026]	0.684	0.512	0.343
MH-MCMC power sampling [Karan and Du, 2025]	0.748	0.573	0.389
Scalable power sampling (SPS) [Ji et al., 2026]	0.758	0.604	0.409
APPS (rollout APF)	<b>0.782</b>	0.616	<b>0.429</b>
APPS (learned APF)	0.764	<b>0.640</b>	0.389
APPS (p-only)	0.744	0.622	0.323
GRPO (MATH) [Shao et al., 2025]	0.785 <sup>↓ 0.3</sup>	0.537 <sup>↑ 10.3</sup>	0.399 <sup>↑ 3.0</sup>
<b>Qwen2.5-7B</b>			
Base decoding [Ji et al., 2026]	0.498	0.329	0.278
Low-temp ( $\tau = 1/\alpha$ ) [Ji et al., 2026]	0.628	0.524	0.303
Best-of- $N$ ( $N = 32$ ) [Ji et al., 2026]	0.650	0.609	0.282
MH-MCMC power sampling [Karan and Du, 2025]	0.706	0.622	0.318
Scalable power sampling (SPS) [Ji et al., 2026]	0.708	<b>0.756</b>	0.349
APPS (rollout APF)	<b>0.736</b>	0.610	<b>0.379</b>
APPS (learned APF)	0.734	0.628	0.374
APPS (p-only)	0.726	0.561	0.354
GRPO (MATH) [Shao et al., 2025]	0.740 <sup>↓ 0.4</sup>	0.561 <sup>↑ 19.5</sup>	0.354 <sup>↑ 2.5</sup>
<b>DeepSeek-Math-7B</b>			
Base decoding [Ji et al., 2026]	0.362	0.415	0.333
Low-temp ( $\tau = 1/\alpha$ ) [Ji et al., 2026]	0.366	0.427	<b>0.430</b>
Best-of- $N$ ( $N = 32$ ) [Ji et al., 2026]	0.420	0.433	0.338
MH-MCMC power sampling [Karan and Du, 2025]	0.424	0.470	0.345
Scalable power sampling (SPS) [Ji et al., 2026]	<b>0.464</b>	0.487	0.364
APPS (rollout APF)	0.462	0.512	0.323
APPS (learned APF)	0.456	<b>0.537</b>	0.323
APPS (p-only)	0.454	0.512	0.333
GRPO (MATH) [Shao et al., 2025]	0.492 <sup>↓ 2.8</sup>	0.524 <sup>↑ 1.3</sup>	0.333 <sup>↑ 9.7</sup>

Highlighting is over *training-free* methods only.

APPS rows use the selected  $P = 32$  operating points from Figure 2.

GRPO is a post-training reference; each annotation reports the absolute pass@1 difference (in percentage points) between GRPO and the best training-free method in that block, with the arrow indicating whether the best training-free method is above or below GRPO.

## References

- Seyedarmin Azizi, Erfan Baghaei Potraghloo, Minoo Ahmadi, Souvik Kundu, and Massoud Pedram. Power-smc: Low-latency sequence-level power sampling for training-free llm reasoning. *arXiv preprint arXiv:2602.10273*, 2026.
- Jinze Bai, Shuai Bai, Yunfei Chu, Zeyu Cui, Kai Dang, Xiaodong Deng, Yang Fan, Wenbin Ge, Yu Han, Fei Huang, et al. Qwen technical report. *arXiv preprint arXiv:2309.16609*, 2023.
- Payman Behnam, Yaosheng Fu, Ritchie Zhao, Po-An Tsai, Zhiding Yu, and Alexey Tumanov. Rocketkv: Accelerating long-context llm inference via two-stage kv cache compression. In *International Conference on Machine Learning*, pages 3358–3392. PMLR, 2025.
- Bradley Brown, Jordan Juravsky, Ryan Ehrlich, Ronald Clark, Quoc V Le, Christopher Ré, and Azalia Mirhoseini. Large language monkeys: Scaling inference compute with repeated sampling. *arXiv preprint arXiv:2407.21787*, 2024.
- Mark Chen, Jerry Tworek, Heewoo Jun, Qiming Yuan, Henrique Ponde de Oliveira Pinto, Jared Kaplan, Harri Edwards, Yuri Burda, Nicholas Joseph, Greg Brockman, Alex Ray, Raul Puri, Gretchen Krueger, Michael Petrov, Heidy Khlaaf, Girish Sastry, Pamela Mishkin, Brooke Chan,

- Scott Gray, Nick Ryder, Mikhail Pavlov, Alethea Power, Lukasz Kaiser, Mohammad Bavarian, Clemens Winter, Philippe Tillet, Felipe Petroski Such, Dave Cummings, Matthias Plappert, Fotios Chantzis, Elizabeth Barnes, Ariel Herbert-Voss, William Hebgen Guss, Alex Nichol, Alex Paino, Nikolas Tezak, Jie Tang, Igor Babuschkin, Suchir Balaji, Shantanu Jain, William Saunders, Christopher Hesse, Andrew N. Carr, Jan Leike, Josh Achiam, Vedant Misra, Evan Morikawa, Alec Radford, Matthew Knight, Miles Brundage, Mira Murati, Katie Mayer, Peter Welinder, Bob McGrew, Dario Amodei, Sam McCandlish, Ilya Sutskever, and Wojciech Zaremba. Evaluating large language models trained on code. 2021a. URL <https://arxiv.org/abs/2107.03374>.
- Mark Chen, Jerry Tworek, Heewoo Jun, Qiming Yuan, Henrique Ponde De Oliveira Pinto, Jared Kaplan, Harri Edwards, Yuri Burda, Nicholas Joseph, Greg Brockman, et al. Evaluating large language models trained on code. *arXiv preprint arXiv:2107.03374*, 2021b.
- Karl Cobbe, Vineet Kosaraju, Mohammad Bavarian, Mark Chen, Heewoo Jun, Lukasz Kaiser, Matthias Plappert, Jerry Tworek, Jacob Hilton, Reiichiro Nakano, Christopher Hesse, and John Schulman. Training verifiers to solve math word problems, 2021. URL <https://arxiv.org/abs/2110.14168>.
- Shengyu Feng, Xiang Kong, Shuang Ma, Aonan Zhang, Dong Yin, Chong Wang, Ruoming Pang, and Yiming Yang. Step-by-step reasoning for math problems via twisted sequential monte carlo. In *The Thirteenth International Conference on Learning Representations*, 2025.
- Xidong Feng, Ziyu Wan, Muning Wen, Stephen Marcus McAleer, Ying Wen, Weinan Zhang, and Jun Wang. Alphazero-like tree-search can guide large language model decoding and training, 2024. URL <https://arxiv.org/abs/2309.17179>.
- Jiaxun Gao, Him Wai Ng, and Z Jane Wang. Once-more: Continuous self-correction for large language models via perplexity-guided intervention. In *The Fourteenth International Conference on Learning Representations*.
- Dan Hendrycks, Collin Burns, Saurav Kadavath, Akul Arora, Steven Basart, Eric Tang, Dawn Song, and Jacob Steinhardt. Measuring mathematical problem solving with the math dataset, 2021. URL <https://arxiv.org/abs/2103.03874>.
- Cheng-Ping Hsieh, Simeng Sun, Samuel Kriman, Shantanu Acharya, Dima Rekesh, Fei Jia, and Boris Ginsburg. Ruler: What’s the real context size of your long-context language models? In *First Conference on Language Modeling*, 2024.
- Bingning Huang, Tu Nguyen, and Matthieu Zimmer. Tree-opo: Off-policy monte carlo tree-guided advantage optimization for multistep reasoning. *arXiv preprint arXiv:2509.09284*, 2025a.
- Yuyi Huang, Runzhe Zhan, Lidia S Chao, Ailin Tao, and Derek F Wong. Path drift in large reasoning models: How first-person commitments override safety. In *Proceedings of the 2025 Conference on Empirical Methods in Natural Language Processing*, pages 19613–19627, 2025b.
- Xiaotong Ji, Rasul Tutunov, Matthieu Zimmer, and Haitham Bou Ammar. Scalable power sampling: Unlocking efficient, training-free reasoning for llms via distribution sharpening, 2026. URL <https://arxiv.org/abs/2601.21590>.
- Aayush Karan and Yilun Du. Reasoning with sampling: Your base model is smarter than you think. *arXiv*, 2025.
- Yujia Li, David Choi, Junyoung Chung, Nate Kushman, Julian Schrittwieser, Rémi Leblond, Tom Eccles, James Keeling, Felix Gimeno, Agustin Dal Lago, et al. Competition-level code generation with alphacode. *Science*, 378(6624):1092–1097, 2022.
- Hunter Lightman, Vineet Kosaraju, Yuri Burda, Harrison Edwards, Bowen Baker, Teddy Lee, Jan Leike, John Schulman, Ilya Sutskever, and Karl Cobbe. Let’s verify step by step. 2023. URL <https://arxiv.org/abs/2305.20050>.
- Nelson F Liu, Kevin Lin, John Hewitt, Ashwin Paranjape, Michele Bevilacqua, Fabio Petroni, and Percy Liang. Lost in the middle: How language models use long contexts. *Transactions of the association for computational linguistics*, 12:157–173, 2024.

- Long Ouyang, Jeffrey Wu, Xu Jiang, Diogo Almeida, Carroll Wainwright, Pamela Mishkin, Chong Zhang, Sandhini Agarwal, Katarina Slama, Alex Ray, et al. Training language models to follow instructions with human feedback. *Advances in neural information processing systems*, 35:27730–27744, 2022.
- David Rein, Betty Li Hou, Asa Cooper Stickland, Jackson Petty, Richard Yuanzhe Pang, Julien Dirani, Julian Michael, and Samuel R. Bowman. Gpqa: A graduate-level google-proof Q&A benchmark. In *Proceedings of the Conference on Language Modeling (COLM)*, 2024. URL <https://openreview.net/forum?id=Ti67584b98>.
- Rulin Shao, Shuyue Stella Li, Rui Xin, Scott Geng, Yiping Wang, Sewoong Oh, Simon Shaolei Du, Nathan Lambert, Sewon Min, Ranjay Krishna, et al. Spurious rewards: Rethinking training signals in rlvr. *arXiv preprint arXiv:2506.10947*, 2025.
- Zhihong Shao, Peiyi Wang, Qihao Zhu, Runxin Xu, Junxiao Song, Xiao Bi, Haowei Zhang, Mingchuan Zhang, Y. K. Li, Y. Wu, and Daya Guo. Deepseekmath: Pushing the limits of mathematical reasoning in open language models, 2024. URL <https://arxiv.org/abs/2402.03300>.
- Xiaozhuang Song, Shufei Zhang, and Tianshu Yu. Rekg-mcts: Reinforcing llm reasoning on knowledge graphs via training-free monte carlo tree search. In *Findings of the Association for Computational Linguistics: ACL 2025*, pages 9288–9306, 2025.
- Hanshi Sun, Momin Haider, Ruiqi Zhang, Huitao Yang, Jiahao Qiu, Ming Yin, Mengdi Wang, Peter Bartlett, and Andrea Zanette. Fast best-of-n decoding via speculative rejection. *Advances in Neural Information Processing Systems*, 37:32630–32652, 2024.
- Mirac Suzgun, Nathan Scales, Nathanael Schärli, Sebastian Gehrmann, Yi Tay, Hyung Won Chung, Aakanksha Chowdhery, Quoc V. Le, Ed H. Chi, Denny Zhou, and Jason Wei. Challenging big-bench tasks and whether chain-of-thought can solve them, 2022. URL <https://arxiv.org/abs/2210.09261>.
- Jason Wei, Xuezhi Wang, Dale Schuurmans, Maarten Bosma, Fei Xia, Ed Chi, Quoc V Le, Denny Zhou, et al. Chain-of-thought prompting elicits reasoning in large language models. *Advances in neural information processing systems*, 35:24824–24837, 2022.
- Wei Wu, Zhuoshi Pan, Kun Fu, Chao Wang, Liyi Chen, Yunchu Bai, Tianfu Wang, Zheng Wang, and Hui Xiong. Tokenselect: Efficient long-context inference and length extrapolation for llms via dynamic token-level kv cache selection. In *Proceedings of the 2025 Conference on Empirical Methods in Natural Language Processing*, pages 21275–21292, 2025.
- Yuxi Xie, Kenji Kawaguchi, Yiran Zhao, Xu Zhao, Min-Yen Kan, Junxian He, and Qizhe Xie. Self-evaluation guided beam search for reasoning, 2023. URL <https://arxiv.org/abs/2305.00633>.
- Qiyang Yu, Zheng Zhang, Ruofei Zhu, Yufeng Yuan, Xiaochen Zuo, Yu Yue, Weinan Dai, Tiantian Fan, Gaohong Liu, Lingjun Liu, et al. Dapo: An open-source llm reinforcement learning system at scale. *arXiv preprint arXiv:2503.14476*, 2025.
- Stephen Zhao, Rob Breckelmann, Alireza Makhzani, and Roger Baker Grosse. Probabilistic inference in language models via twisted sequential monte carlo. In *International Conference on Machine Learning*, pages 60704–60748. PMLR, 2024.

## A Extended Related Work

**Post training and verifier based reasoning.** A major driver of recent reasoning gains is post training with preference [Ouyang et al., 2022] or reward optimization [Shao et al., 2024, Huang et al., 2025a, Yu et al., 2025]. In parallel, verifier based pipelines improve reliability by sampling multiple solutions and selecting using an outcome reward model or a process reward model, with the strongest variants relying on step level supervision and careful reward design. These approaches can be highly effective, but they introduce training pipelines and often depend on additional supervision signals or verifier models.

**Training free inference time search for reasoning.** A complementary line of work improves reasoning without updating the base model by changing how we sample. Local sharpening methods [Karan and Du, 2025] such as low temperature sampling are nearly free but remain myopic, while selection based methods such as Best-of-N [Brown et al., 2024, Sun et al., 2024] improve by exploiting sample diversity but still score candidates using the base model. More structured inference time search methods explore multiple trajectories through sampling and selection [Song et al., 2025, Feng et al., 2024, Xie et al., 2023]. This paper belongs to the training free direction, and targets sequence level sharpening rather than token level heuristics.

**Power distributions and finite budget approximations.** Power sampling [Karan and Du, 2025] formalizes sequence level sharpening by targeting  $\pi_\alpha(x) \propto p(x)^\alpha$ . Early practical realizations use Markov chain Monte Carlo updates over long trajectories, which can be statistically principled but typically incur large wall clock overhead due to repeated suffix regeneration. Recent scalable approximations [Ji et al., 2026] replace iterative mixing with explicit lookahead and rollout estimation of future dependent factors, improving finite budget behavior but shifting cost toward candidate wise fan out at decision points. Closely related work, such as Power-SMC [Azizi et al., 2026], uses sequential Monte Carlo with resampling and cache reordering to achieve strong accuracy–latency trade-offs under large particle counts and shorter generation caps in latency-focused settings. Our method adopts the same particle perspective, but differs in where control enters inference: Power SMC centers the proposal, whereas APPS centers weighted selection under a finite population budget. In its minimal form, APPS already defines a strong blockwise particle sampler; richer future-value selection potentials then refine resampling without altering the underlying propagation law.

**Twisted and value guided particle methods for LLMs.** Several recent works [Zhao et al., 2024, Feng et al., 2025] bring twisted sequential Monte Carlo ideas into LLM reasoning, often by introducing stepwise potentials that encourage trajectories with higher expected downstream reward or verifier scores. Feng et al. [2025] applies twisted SMC to math reasoning by estimating expected future rewards of partial solutions and using this signal to focus sampling on promising candidates. These methods highlight the importance of future value signals for long horizon reasoning. Our approach uses a related future-aware principle, but differs in where the signal enters: propagation remains proposal-aware and stable, while future value acts only through resampling. This lets the same inference law range from a strong p-only backbone to more explicit rollout or learned selection-time value estimates.

## B Algorithm

Unlike token-level SMC schemes, APPS places the inference problem at the level of blockwise propagation and selection under a finite particle budget. Its base sampler already targets the sequence-level power objective through proposal-corrected weighting, while rollout and learned selection potentials intervene only in the redistribution of particle mass across prefixes.

---

**Algorithm 1 Our method, (APPS).** A blockwise particle sampler for the sequence-level power objective. The base sampler propagates a bounded population of prefixes, applies proposal-corrected power weighting, and redistributes finite particle mass by ESS-gated resampling. rollout and learned selection potentials refine only the selection step.

---

**Input:** prompt  $x_0$ , base LM  $p$ , power  $\alpha > 1$ , particle budget cap  $P_{\max}$ , block size  $B$ , proposal family  $\{q_j(\cdot | \cdot)\}$

**Input:** APF mode  $\in \{\text{none}, \text{rollout}, \text{learned}\}$ ; rollout budget  $(R, H)$  if `rollout`

**Output:** final particle by sampling or score-based selection

- 1: **Initialize population**
- 2: Set active population size  $P_1 \leq P_{\max}$
- 3: Set particles  $x^{(i)} \leftarrow x_0$  and incremental log-weights  $\log w^{(i)} \leftarrow 0$  for  $i = 1, \dots, P_1$
- 4: Set block index  $j \leftarrow 1$
- 5: **while** not terminated **do**
- 6:   **Propagate one block per particle**
- 7:   **for**  $i \leftarrow 1$  to  $P_j$  **do**
- 8:     Store current prefix  $x_{\text{prev}}^{(i)} \leftarrow x^{(i)}$
- 9:     Sample block  $[b_j]^{(i)} \sim q_j(\cdot | x^{(i)})$
- 10:     Extend particle prefix  $x^{(i)} \leftarrow x^{(i)} \oplus [b_j]^{(i)}$
- 11:   **end for** ▷ advance a bounded population of prefixes
- 12:   **Apply proposal-corrected power weighting**
- 13:   **for**  $i \leftarrow 1$  to  $P_j$  **do**
- 14:      $\log w^{(i)} \leftarrow \log w^{(i)} + \alpha \log p([b_j]^{(i)} | x_{\text{prev}}^{(i)}) - \log q_j([b_j]^{(i)} | x_{\text{prev}}^{(i)})$
- 15:   **end for** ▷ preserve the sequence-level power target
- 16:   **Form selection weights**
- 17:   Set  $\log \tilde{w}^{(i)} \leftarrow \log w^{(i)}$  for all  $i = 1, \dots, P_j$
- 18:   **if** APF mode = `rollout` **and** resampling is imminent **then**
- 19:     **if** APF mode = `rollout` **then**
- 20:       Estimate  $\log \psi^{(i)}$  by  $R$  rollouts of horizon  $H$  from  $x^{(i)}$
- 21:     **else if** APF mode = `learned` **then**
- 22:       Predict  $\log \psi^{(i)}$  from the boundary representation  $h_{\text{last}}(x^{(i)})$
- 23:     **end if**
- 24:     Refine selection weights:  $\log \tilde{w}^{(i)} \leftarrow \log \tilde{w}^{(i)} + \eta \log \psi^{(i)}$  for all  $i = 1, \dots, P_j$  ▷ future value
- 25:   **enters only here**
- 26:   **end if**
- 27:   **Reallocate finite particle budget**
- 28:   Set next population size  $P_{j+1} \leq P_{\max}$  from boundary ambiguity ▷ shift budget toward unresolved prefixes
- 29:   **Resample if the population has collapsed**
- 30:   Compute ESS from  $\{\log \tilde{w}^{(i)}\}_{i=1}^{P_j}$
- 31:   **if** ESS  $< \kappa P_j$  **then**
- 32:     Sample ancestor indices  $a_{1:P_{j+1}} \sim \text{RESAMPLE}(\propto \exp(\log \tilde{w}^{(i)}))$
- 33:     (ablated variant) keep elite particle in the resampled set
- 34:     Replace particles:  $x^{(i)} \leftarrow x^{(a_i)}$  for  $i = 1, \dots, P_{j+1}$
- 35:     Reset incremental log-weights  $\log w^{(i)} \leftarrow 0$  for  $i = 1, \dots, P_{j+1}$
- 36:   **end if**
- 37:   **Advance to the next boundary**
- 38:    $j \leftarrow j + 1$
- 39: **end while**
- 40: **return** final particle by sampling from  $\exp(\log w)$  or selecting the best score

---

## C Proofs for Section 3

### C.1 Proof of Theorem 1 (Future-value factorization)

*Proof.* By definition,

$$\pi_J(b_{1:J} | x) = \frac{1}{Z_J(x)} \prod_{k=1}^J p(b_k | x, b_{<k})^\alpha.$$

Fix a boundary  $j \leq J$ . Then

$$\pi_{1:j}(b_{1:j} | x) = \sum_{b_{j+1:J}} \pi_J(b_{1:J} | x) = \frac{1}{Z_J(x)} \sum_{b_{j+1:J}} \prod_{k=1}^J p(b_k | x, b_{<k})^\alpha.$$

Split the product into prefix and suffix terms:

$$\prod_{k=1}^J p(b_k | x, b_{<k})^\alpha = \left( \prod_{k=1}^j p(b_k | x, b_{<k})^\alpha \right) \left( \prod_{k=j+1}^J p(b_k | x, b_{<k})^\alpha \right).$$

The prefix factor is constant with respect to the sum over  $b_{j+1:J}$ , so

$$\pi_{1:j}(b_{1:j} | x) = \frac{1}{Z_J(x)} \left( \prod_{k=1}^j p(b_k | x, b_{<k})^\alpha \right) \sum_{b_{j+1:J}} \prod_{k=j+1}^J p(b_k | x, b_{<k})^\alpha = \frac{\gamma_j(b_{1:j} | x) z_{j+1}(x, b_{1:j})}{Z_J(x)},$$

which proves (5). For the conditional law, divide the prefix marginal at level  $j$  by the one at level  $j-1$ :

$$\pi_j(b_j | x, b_{<j}) = \frac{\pi_{1:j}(b_{1:j} | x)}{\pi_{1:j-1}(b_{<j} | x)} = \frac{\gamma_j(b_{1:j} | x) z_{j+1}(x, b_{1:j})}{\gamma_{j-1}(b_{<j} | x) z_j(x, b_{<j})}.$$

Since  $\gamma_j(b_{1:j} | x) = \gamma_{j-1}(b_{<j} | x) p(b_j | x, b_{<j})^\alpha$ , this gives (6).  $\square$

## C.2 Proof of Theorem 2 (Bounded-test particle approximation)

*Proof.* To simplify notation, write  $\pi := \pi_j$  and  $q := q_j$ . Let

$$r(x) := \frac{d\pi}{dq}(x).$$

Then

$$\mathbb{E}_q[r(X)] = 1, \quad \mathbb{E}_q[r(X)^2] = 1 + \chi^2(\pi||q).$$

Let  $X_1, \dots, X_P \stackrel{\text{i.i.d.}}{\sim} q$ , set

$$r_i := r(X_i), \quad S := \sum_{i=1}^P r_i, \quad \bar{w}_i := \frac{r_i}{S}.$$

Fix any measurable  $f$  with  $\|f\|_\infty \leq 1$ , and write

$$\mu := \pi(f) = \int f d\pi = \mathbb{E}_q[r(X)f(X)].$$

The SNIS estimator is

$$\hat{\pi}^P(f) = \sum_{i=1}^P \bar{w}_i f(X_i) = \frac{\sum_{i=1}^P r_i f(X_i)}{S}.$$

Hence

$$\hat{\pi}^P(f) - \mu = \frac{\sum_{i=1}^P r_i (f(X_i) - \mu)}{S}.$$

Define

$$Z_i := r_i (f(X_i) - \mu), \quad N := \sum_{i=1}^P Z_i.$$

Then

$$\hat{\pi}^P(f) - \mu = \frac{N}{S}.$$

First,  $\mathbb{E}[Z_i] = 0$ , because

$$\mathbb{E}[Z_i] = \mathbb{E}_q[r(X)(f(X) - \mu)] = \mathbb{E}_q[r(X)f(X)] - \mu \mathbb{E}_q[r(X)] = \mu - \mu = 0.$$

Also, since  $\|f\|_\infty \leq 1$ , we have  $|\mu| \leq 1$ , hence  $|f(X_i) - \mu| \leq 2$ . Therefore

$$Z_i^2 = r_i^2 (f(X_i) - \mu)^2 \leq 4r_i^2,$$

and so

$$\mathbb{E}[Z_i^2] \leq 4\mathbb{E}_q[r(X)^2] = 4(1 + \chi^2(\pi\|q)).$$

Because the  $Z_i$  are independent and mean zero,

$$\mathbb{E}[N^2] = \sum_{i=1}^P \mathbb{E}[Z_i^2] \leq 4P(1 + \chi^2(\pi\|q)).$$

By Cauchy–Schwarz,

$$\mathbb{E}|N| \leq \sqrt{\mathbb{E}[N^2]} \leq 2\sqrt{P} \sqrt{1 + \chi^2(\pi\|q)}.$$

Next, since  $S = \sum_{i=1}^P r_i$  and  $\mathbb{E}_q[r] = 1$ ,

$$\mathbb{E}[S] = P.$$

Also,

$$\text{Var}(r) = \mathbb{E}_q[r^2] - 1 = \chi^2(\pi\|q),$$

so

$$\text{Var}(S) = P \chi^2(\pi\|q).$$

Let

$$E := \{S > P/2\}.$$

By Chebyshev's inequality,

$$\mathbb{P}(E^c) = \mathbb{P}\left(S \leq \frac{P}{2}\right) = \mathbb{P}\left(S - P \leq -\frac{P}{2}\right) \leq \frac{4 \text{Var}(S)}{P^2} = \frac{4\chi^2(\pi\|q)}{P}.$$

We now split on  $E$ :

$$\mathbb{E}|\hat{\pi}^P(f) - \mu| = \mathbb{E}\left[\left|\frac{N}{S}\right| \mathbf{1}_E\right] + \mathbb{E}\left[\left|\frac{N}{S}\right| \mathbf{1}_{E^c}\right].$$

On  $E$ , we have  $1/S \leq 2/P$ , hence

$$\mathbb{E}\left[\left|\frac{N}{S}\right| \mathbf{1}_E\right] \leq \frac{2}{P} \mathbb{E}|N| \leq \frac{4}{\sqrt{P}} \sqrt{1 + \chi^2(\pi\|q)}.$$

On  $E^c$ , we use the deterministic bound

$$|N| = \left| \sum_{i=1}^P r_i (f(X_i) - \mu) \right| \leq \sum_{i=1}^P r_i |f(X_i) - \mu| \leq 2 \sum_{i=1}^P r_i = 2S,$$

which implies  $|N/S| \leq 2$ . Therefore

$$\mathbb{E}\left[\left|\frac{N}{S}\right| \mathbf{1}_{E^c}\right] \leq 2\mathbb{P}(E^c) \leq \frac{8\chi^2(\pi\|q)}{P}.$$

Combining the two bounds proves (7). □

### C.3 Proof of Proposition 1 (Variance reduction from future-value selection)

*Proof.* By definition of the  $\chi^2$ -divergence,

$$1 + \chi^2(\pi_j\|\tilde{q}_j) = \sum_{b_j} \frac{\pi_j(b_j)^2}{\tilde{q}_j(b_j)}.$$

Let  $C := \sum_{b'} q_j(b') \psi(b') = \mathbb{E}_{q_j}[\psi(b_j)]$  act as the normalizer constant. Substituting the definition of the effective proposal  $\tilde{q}_j(b_j) = q_j(b_j) \psi(b_j)/C$  and the ratio  $r(b_j) = \pi_j(b_j)/q_j(b_j)$ , we obtain:

$$\begin{aligned} 1 + \chi^2(\pi_j \|\tilde{q}_j) &= \sum_{b_j} \frac{\pi_j(b_j)^2 C}{q_j(b_j) \psi(b_j)} \\ &= C \sum_{b_j} q_j(b_j) \frac{r(b_j)^2}{\psi(b_j)} \\ &= \mathbb{E}_{q_j}[\psi(b_j)] \mathbb{E}_{q_j} \left[ \frac{r(b_j)^2}{\psi(b_j)} \right]. \end{aligned}$$

We now frame this product of expectations using the general definition of covariance. For any two random variables  $U$  and  $W$  under a probability distribution  $q_j$ , it holds that  $\text{Cov}_{q_j}(U, W) = \mathbb{E}_{q_j}[UW] - \mathbb{E}_{q_j}[U] \mathbb{E}_{q_j}[W]$ .

Setting  $U := \psi(b_j)$  and  $W := r(b_j)^2/\psi(b_j)$ , we observe that their product trivially simplifies inside the expectation to  $UW = r(b_j)^2$ . Therefore:

$$\text{Cov}_{q_j} \left( \psi(b_j), \frac{r(b_j)^2}{\psi(b_j)} \right) = \mathbb{E}_{q_j}[r(b_j)^2] - \mathbb{E}_{q_j}[\psi(b_j)] \mathbb{E}_{q_j} \left[ \frac{r(b_j)^2}{\psi(b_j)} \right].$$

Rearranging this equation immediately yields Identity (13):

$$1 + \chi^2(\pi_j \|\tilde{q}_j) = \mathbb{E}_{q_j}[r(b_j)^2] - \text{Cov}_{q_j} \left( \psi(b_j), \frac{r(b_j)^2}{\psi(b_j)} \right).$$

In the baseline scenario without a future-value selection potential ( $\psi \equiv 1$ ), the covariance term is trivially 0 (since variance/covariance with a constant is zero), evaluating to exactly  $1 + \chi^2(\pi_j \|\tilde{q}_j) = \mathbb{E}_{q_j}[r(b_j)^2]$ . By substituting this definition into the identity, the difference between the divergences is precisely the isolated covariance:

$$\chi^2(\pi_j \|\tilde{q}_j) = \chi^2(\pi_j \|\tilde{q}_j) - \text{Cov}_{q_j} \left( \psi(b_j), \frac{r(b_j)^2}{\psi(b_j)} \right).$$

Hence, a strict variance reduction  $\chi^2(\pi_j \|\tilde{q}_j) < \chi^2(\pi_j \|\tilde{q}_j)$  occurs if and only if the covariance is strictly positive.

Finally, in the ideal limit where  $\psi(b_j) \propto r(b_j)$ , we have  $r(b_j) = k\psi(b_j)$  for some scalar constant  $k$ . Then  $W = k^2\psi(b_j) \propto U$ . The positive correlation is maximized asymptotically, and directly applying the substitution into  $\tilde{q}_j$  provides  $\tilde{q}_j(b_j) = kq_j(b_j)\psi(b_j)/(kC) = \pi_j(b_j)$ , rendering the target and effective proposal equal and trivially giving  $\chi^2(\pi_j \|\tilde{q}_j) = 0$ .  $\square$

#### C.4 Corollary 1: Minimal APPS as proposal-corrected importance sampling

**Corollary 1** (Minimal APPS as proposal-corrected blockwise importance sampling). *Consider a sequential block proposal*

$$q(b_{1:J} | x) = \prod_{j=1}^J q_j(b_j | x, b_{<j}).$$

*Then the cumulative importance weight produced by the proposal-corrected update*

$$\Delta \log w_j = \alpha \log p(b_j | x, b_{<j}) - \log q_j(b_j | x, b_{<j})$$

*satisfies*

$$W_J(b_{1:J}) := \prod_{j=1}^J \frac{p(b_j | x, b_{<j})^\alpha}{q_j(b_j | x, b_{<j})} = \frac{\gamma_J(b_{1:J} | x)}{q(b_{1:J} | x)}. \quad (17)$$

*Hence the minimal APPS sampler defines the standard blockwise importance-sampling construction for the sequence-level power target (4); with standard ESS-gated resampling, this becomes the corresponding blockwise SMC approximation.*

*Proof.* Summing the incremental log-weights gives

$$\sum_{j=1}^J \Delta \log w_j = \sum_{j=1}^J \log \frac{p(b_j | x, b_{<j})^\alpha}{q_j(b_j | x, b_{<j})} = \log \prod_{j=1}^J \frac{p(b_j | x, b_{<j})^\alpha}{q_j(b_j | x, b_{<j})}.$$

Exponentiating yields

$$W_J(b_{1:J}) = \prod_{j=1}^J \frac{p(b_j | x, b_{<j})^\alpha}{q_j(b_j | x, b_{<j})}.$$

Using the definitions of  $\gamma_J$  and the sequential proposal factorization,

$$\gamma_J(b_{1:J} | x) = \prod_{j=1}^J p(b_j | x, b_{<j})^\alpha, \quad q(b_{1:J} | x) = \prod_{j=1}^J q_j(b_j | x, b_{<j}),$$

which proves (17).  $\square$

**Discussion and scope.** Theorem 1 is the conceptual centerpiece: it shows that future value is exactly the missing factor in the true block-boundary marginal. Theorem 2 then gives a correct finite- $P$  approximation guarantee for bounded observables, avoiding a support-free total-variation claim over all measurable sets. Corollary 1 formalizes that the proposal-corrected minimal APPS backbone is already a valid blockwise importance-sampling / SMC construction for the sequence-level power target.

**Important note on APF selection potentials.** The target-preservation statement in Corollary 1 applies to the minimal proposal-corrected sampler. If one resamples using modified selection weights proportional to  $w_j^{(i)} \psi_j^{(i)\eta}$ , then preserving the same underlying target generally requires an explicit auxiliary-SMC correction. Without such a correction, the modified resampling law should be interpreted as a finite-budget selection heuristic rather than an exact target-preserving transformation.

## D Rollout and learned selection potentials

We describe the two practical realizations of the selection potential in (10). In rollout APF, the future-value signal is computed directly from short lookahead launched from the current prefixes. In learned APF, the same signal is amortized by a lightweight predictor evaluated at the same resampling boundaries while keeping the base language model fixed.

### D.1 Boundary-level supervision

Rollout supervision is collected at resampling boundaries. For each candidate prefix evaluated at boundary  $j$ , we store

$$(h_j^{(i)}, y_j^{(i)}, g_j^{(i)}), \quad y_j^{(i)} := \log \psi_j^{(i)},$$

where  $h_j^{(i)} \in \mathbb{R}^d$  is the boundary representation,  $y_j^{(i)}$  is the rollout-based selection potential, and  $g_j^{(i)}$  identifies the corresponding boundary group. All examples with the same group identifier arise from the same resampling decision.

The group structure is fundamental. In a particle system, future value matters only through how selection redistributes representation within a boundary group. We therefore preserve groups across shard merging, with an ablated filter for degenerate groups if needed, and split train/validation data by group. To reduce avoidable variance, rollout targets are generated with a deterministic seeding policy during data construction.

### D.2 Effective training target

The learned head is trained to predict the signal actually used at decode time. Let  $g$  denote a boundary group and let  $y^{(i)}$  be the raw rollout score for candidate  $i \in g$ . The effective target is

$$\tilde{y}^{(i)} = \eta \cdot \text{clip} \left( y^{(i)} - \frac{1}{|g|} \sum_{k \in g} y^{(k)} \right), \quad (18)$$

with the obvious simplifications when centering or clipping is disabled.

This centering makes the target explicitly boundary-relative: additive offsets within a group are irrelevant, because selection depends only on how prefixes compete for representation at the same resampling boundary. Equivalently, the learned target is defined only up to within-boundary competition: what matters is not the absolute scale of future value, but how it tilts selection probabilities and expected offspring within the current population.

We considered two target parameterizations. *Standardized-target distillation* predicts globally normalized rollout scores and relies on the loss to recover boundary structure. Our main formulation, *decode-aligned distillation*, predicts the effective target in (18) directly. Unless noted otherwise, the learned-APF results in the main text use decode-aligned distillation.

### D.3 Head and objective

The learned selection potential is produced by a lightweight multilayer perceptron

$$f_{\theta} : \mathbb{R}^d \rightarrow \mathbb{R},$$

applied to the boundary representation  $h_j^{(i)}$ . Since the learned potential is used only through selection within a boundary, the objective emphasizes relative fidelity within groups rather than absolute calibration across unrelated boundaries.

For decode-aligned distillation, let  $\hat{y}^{(i)}$  denote the student prediction after applying the same group-wise centering, clipping, and scaling used in decoding. The training loss is a weighted sum of:

1. a smooth- $L_1$  regression term between  $\hat{y}$  and  $\tilde{y}$ ;
2. a group-centered regression term;
3. a listwise distillation term matching the rollout and learned softmax distributions within each boundary;
4. a within-group pairwise ranking loss; and
5. a top-1 cross-entropy term matching the winning prefix selected by rollout APF.

Group weights are derived from the rollout signal, assigning larger weight to boundaries with larger within-group spread or winner–runner-up margin. These terms all target the same object from different angles: not the absolute value of a prefix in isolation, but its role in the boundary-level competition for survival and offspring.

### D.4 Optimization and model selection

We train with AdamW and cosine annealing. Minibatches are formed from whole groups rather than independent rows, since the structured losses are defined over candidates from the same boundary. We also maintain an exponential moving average of parameters for evaluation.

Held-out evaluation is group-aware. In addition to pointwise error, we compute group top-1 agreement, group pairwise accuracy, and Pearson correlation with rollout effective scores. Checkpoints are selected primarily by group top-1 agreement, with group pairwise accuracy used as a tie-breaker. This matches the intended role of the learned head: improving resampling decisions rather than fitting raw rollout values.

### D.5 Summary

The learned APF head is trained to imitate the effective rollout signal used by APPS at resampling time. The construction is group-aware throughout: supervision is collected at resampling boundaries, objectives model competition within a boundary, batching preserves boundary structure, and checkpoint selection is based on boundary-level selection quality.

## E Blockwise execution, cache reuse, and dynamic allocation

**Blockwise execution and KV reuse.** APPS is formulated at the block level but executed through a streaming KV-cache path. The model is evaluated once on the prompt, after which decoding proceeds

token by token while maintaining one KV cache per particle; at resampling boundaries, caches are reordered according to the selected ancestors, analogous to beam search. The method is thus blockwise in logic but streaming in execution.

### E.1 Finite-budget population reallocation

Under dynamic allocation, APPS updates the active population size only at block boundaries. The underlying idea is simple: boundaries that remain unresolved should retain more particle mass, while collapsed boundaries should release budget.

Let  $\{\log \tilde{w}_j^{(i)}\}_{i=1}^{P_j}$  denote the selection scores at boundary  $j$ , after any rollout or learned selection potential has been incorporated. We summarize boundary uncertainty by an ambiguity score  $a_j \in [0, 1]$ . In practice, we use a simple signal derived either from the top-one/top-two gap or from the entropy of the normalized selection weights. A representative entropy-based form is

$$\bar{\pi}_j^{(i)} = \frac{\exp(\log \tilde{w}_j^{(i)})}{\sum_{k=1}^{P_j} \exp(\log \tilde{w}_j^{(k)})}, \quad a_j = \frac{-\sum_{i=1}^{P_j} \bar{\pi}_j^{(i)} \log \bar{\pi}_j^{(i)}}{\log P_j}.$$

Large  $a_j$  indicates a diffuse, unresolved population; small  $a_j$  indicates that selection mass is already concentrated.

The next active population size is then chosen by a monotone budget-allocation rule,

$$P_{j+1} = g(a_j; P_{\min}, P_{\max}), \quad P_{\min} \leq P_{j+1} \leq P_{\max},$$

where  $g$  increases with ambiguity. In our implementation, this is realized as a clipped linear map,

$$P_{j+1} = \text{clip}(P_{\min} + \lfloor (P_{\max} - P_{\min}) a_j \rfloor, P_{\min}, P_{\max}),$$

and the updated budget is realized at the next resampling step. Thus dynamic allocation does not alter the proposal or weighting rule; it changes only how much particle mass remains active at subsequent boundaries.

To characterize this mechanism empirically, we report several boundary-level diagnostics: the average active population over blocks,

$$\bar{P} = \frac{1}{J} \sum_{j=1}^J P_j,$$

the fraction of blocks at minimum population,

$$\frac{1}{J} \sum_{j=1}^J \mathbf{1}\{P_j = P_{\min}\},$$

the mean ambiguity fraction,

$$\bar{a} = \frac{1}{J} \sum_{j=1}^J a_j,$$

the mean absolute change in active population size,

$$\frac{1}{J-1} \sum_{j=1}^{J-1} |P_{j+1} - P_j|,$$

the number of allocation increases and decreases, and the average number of unique ancestors after resampling. Together, these diagnostics distinguish runs that are merely faster from runs that genuinely reallocate finite compute toward unresolved regions without collapsing useful diversity.

**Scores across resampling events.** We maintain two notions of score. The first is a local selection score, derived from the incremental weight since the last resampling step and used to form the resampling distribution at the current boundary. The second is a cumulative ancestry score, copied through sampled parent indices and kept comparable across resampling events for final particle selection. This keeps local resampling decisions numerically stable while retaining a trajectory-level score for final selection across resampling events.

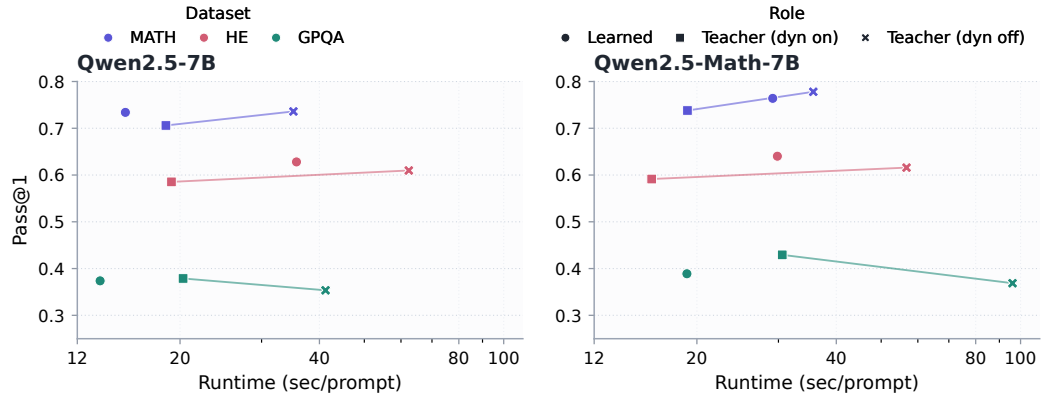


Figure 3: **Wall-clock runtime–accuracy trade-offs for learned and rollout APF.** Each point is a completed full-benchmark run, plotted by runtime per prompt and pass@1. Dynamic allocation substantially reduces rollout APF runtime, mainly acting as a compute-control mechanism. Learned APF gives the strongest overall speed–accuracy trade-off on MATH500 and HumanEval, while the corrected GPQA runs show rollout APF attaining higher pass@1 at higher wall-clock cost. Overall, learned APF is the more efficient future-value estimator, whereas rollout APF can be more accurate when its online estimates justify the extra compute.

## E.2 Further runtime–accuracy analysis under dynamic allocation

Figure 3 gives a complementary view of how dynamic allocation changes the runtime–accuracy frontier, with particular emphasis on the relative operating regions of learned APF and teacher APF.